Desalination and Water Treatment
www.deswater.com

doi: 10.5004/dwt.2020.25847

195 (2020) 114–127
August

Adsorption of humic acid from seawater on organo Mg–Fe-layered double hydroxides: isotherm, kinetic modeling, and ionic strength

K. Bouarouri[a], M.W. Naceur[a], S. Hanini[b], S. Soukane[a], M. Laidi[b], N. Drouiche[c,*]

[a]*Laboratoire Eau, Environnement, et Developpement Durable (2E2D), Chemical Engineering Department, Blida1 University, BP 270 Blida, Algeria*
[b]*Biomaterials and Transport Phenomena Laboratory (LBMPT), Médéa University, 26000 Médéa, Algeria*
[c]*Centre de Recherche en Technologie des Semi-Conducteurs pour l'Energétique, 2 Bd Frantz Fanon BP140 Alger-7-merveilles, 16038 Alger, Algeria, email: nadjibdrouiche@yahoo.fr (N. Drouiche)*

Received 20 November 2019; Accepted 17 March 2020

ABSTRACT

The aim of this study is to bring an in-depth understanding of the adsorption phenomenon of humic acid onto calcined layered double hydroxides (LDH) and organophilic LDH in seawater. LDHs were prepared by co-precipitation at constant pH with a molar ration M^{+2}/M^{+3} = 2. Organophilic LDH were prepared by interposing a surfactant (sodium dodecylsulfate, SDS 0.1 M). All samples were characterized using X-ray diffraction, Fourier transform infrared spectrometry, Brunauer–Emmett–Teller method, and scanning electron microscopy. Several adsorption kinetics models (pseudo-first-order, pseudo-second-order, *n*th-order, and intraparticle diffusion) were tested against the experimental results. The calculation of the corresponding parameters shows that results are best fitted with the *n*th-order ($n \in R^+$) $n \neq 1$ model with a determination coefficient close to 1 and a relatively small root mean square error. Among the available mathematical models used to describe the isotherms experimental results (Langmuir, Freundlich, Sips, and many-parameters models). The six models that are proposed show a better performance than Freundlich, Langmuir, and Sips. The calculation of the parameters of the different adsorption models was performed on MATLAB using genetic algorithms. Thermodynamic analysis of sorption isotherms suggests that sorption process of humic acid is spontaneous ($\Delta G° < 0$), with a positive enthalpy variation, characteristic of an endothermic process. The positive entropy variation indicates a disorder increase at the solid-solution interface during humic acid sorption. The values of the effective diffusion coefficient and energy activation deduced by modeling range between (10^{-13}–10^{-9}) m^2/s and E_a = (28–33) kJ/mol, respectively, as reported in the literature. The materials prepared showed an excellent regeneration ability and were successfully reused after several adsorption cycles.

Keywords: Adsorption; LDH; Humic acid; Seawater; Anionic surfactant; Organophilization

I. Introduction

Seawater contains mineral and organic compounds either emanating from both animal and vegetal life or produced by chemical synthesis [1]. Among natural organic compounds are humic species, mainly consisting of humic and fulvic acids that represent the major vector of toxic species such as heavy metals and pesticides [2,3]. Humic acids have a strong effect on the properties of natural water since they represent most of the dissolved organic matter [4] with 50%–90% of dissolved organic carbon [5]. These molecules

* Corresponding author.

affect the taste and color of water [6], and represent a source of nutrients to bacteria and trap heavy metals, pesticides, and herbicides [3]. Moreover, the reaction between humic acids and chlorine during water treatment produces carcinogenic compounds [7]. Humic acids have a negative charge in aqueous solutions due to the presence of carboxylic and phenolic functions [8,9]. Several physical, chemical, and biological processes have been used to eliminate humic compounds such as coagulation, flocculation, precipitation, oxidation, and adsorption [10]. Among these techniques, adsorption is popular due to its advantages of easy operation, high efficiency, low cost, and reusability [11,12]. However, adsorption has certain limitations also, such as it could not achieve a good status at commercial levels due to the lack of suitable adsorbents of high adsorption capacity and unavailability of commercial scale columns. Moreover, the design of suitable adsorbent, which has good performance, should be considered as a crucial stage. Recent use of anionic clays (layered double hydroxides (LDH)) as adsorbents showed a particular interest in the elimination of micro-pollutants [13]. LDH have a brucite layer structure [14] where the brucitic layers ($M_{II}(OH)_2$) are positively charged. This is due to the partial substitution of bivalent cations M^{II} by trivalent cations M^{III} [15]. Electroneutrality is ensured by anionic species, which are solvated by water molecules present in sheets interspace [13]. The lamellar structure enhances ionic exchanges of these compounds, thus broadening their range of applicability (catalysis, environment, pharmaceutical) [16]. These anionic clays were the topic of numerous investigations for their physical and chemical properties. The calcined phase of the anionic clay has been widely used as an adsorbant [17]. The insertion of anionic surfactants modifies the hydrophilic property of the clay which becomes hydrophobic and capable of adsorbing organic pollutants [18]. Anionic clays have been used as adsorbants in environmental applications. Li et al. [19] focused on the adsorption tests of humic acid on calcined and non-calcined Magnetic Zn/Al LDH (M Zn/Al LDH). They showed that the adsorption capacity of calcined LDH, equal to 80 mg/g, is higher than that of non-calcined LDH, equal to 49.15 mg/g. This study revealed that M Zn/Al CLDH was an effective adsorbent for HA removal in water treatment. Zermane et al. [20] investigate and compare the efficiency of three adsorbents toward the adsorption of Basic Yellow 28 both in single and binary mixture systems where the influence of humic acid as co-adsorbate on the sorption parameters was examined. The adsorbents investigated in this study were as follows: (i) an iron organo–inorgano pillared clay (Fe-SMPM); (ii) goethite and hydrous ferric oxide, two synthetic iron (oxy) hydroxides. Humic acid is organic matter with various functional groups, extensive sources and has been considered as an adsorbent for heavy metal removal. Heat-treated humic acid/MgAl-layered double hydroxide composite (HA/MgAl-LDH) was fabricated by Xiang et al. [21] through a coprecipitation method and used as an adsorbent for the removal of Cd in aqueous solution. The maximum theoretical adsorption capacity calculated for Cd was 155.28 mg/g. The synthesis of a humic acid-layered double hydroxide (HA-LDH) hybrid was purposed by Shi et al. [22] for the remediation of contaminated soils in mining area. In order to investigate the effect of HA-LDH on the mine soil, greenhouse experiments of Artemisia ordosica were carried out under different concentrations of amendments. By The HA-LDH and *Artemisia ordosica* could effectively decrease the bioavailability of heavy metals (such as Pb, Cr, Ni, Cd, Zn, and As) in the mine soil, and improve the enzyme activities of β-glucosidase, urease, and phosphatase. The authors conclude that the calcined phase has a higher adsorption capacity (375 mg/g) compared to the non-calcined phase. The elimination of Congo red, an anionic dye, by an anionic clay of Mg–Al type has been investigated by Lafi et al. [23]. The authors conclude that the adsorption kinetics correspond to a pseudo-second-order model and the isotherms to Langmuir model. They suggest that electrostatic attraction controls the adsorption of Congo red on Mg–Al phase. Chitrakar et al. [24] studied the adsorption of seawater phosphate on hydrotalcite of Mg–Mn-300 type obtained after calcination at 573 K with a molar ratio of 3. Moreover, the adsorbent exhibits a high chemical stability during adsorption–desorption cycle since it retains a high phosphate adsorption after several cycles. It can be concluded that hydrotalcites (LDH) are efficient adsorbents for depollution. In the present work, SDS based organophilic LDH, calcined at 773 K are used for the elimination of humic acid from seawater. A particular interest is given to the investigation of kinetic and thermodynamic equilibrium as well as adsorption thermodynamics to provide a description of the fixation mode using recently proposed multi-parameters adsorption models.

2. Materials and methods

2.1. Materials

Sodium dodecylsulfate (SDS, 0.1 M), HCL (0.1 M), NaOH (0.1 M), $MgCl_2{\cdot}6H_2O$, Na_2CO_3, and $FeCl_3{\cdot}6H_2O$. All reactants from Panreac Qimica SA Castellar del Valles Barcelona, Espana.

2.2. Preparation of adsorbents

2.2.1. Synthesis of Mg–Fe–CO_3 phase

Mg–Fe phase with a ratio of Mg/Fe = 2 was prepared by adding a basic solution of NaOH (2 M) and Na_2CO_3 (1 M) to a mixture of two salts, namely $MgCl_2{\cdot}6H_2O$ (0.66 M) and $FeCl_3{\cdot}6H_2O$ (0.33 M). Optimum parameters that would lead to crystallized LDH consist of pH = 10, a temperature of 298 K, and a mixing time of 6 h. The resulting suspension is mixed overnight to enhance material crystallization followed by washing, drying at 338 K, and grinding to obtain Mg–Fe–CO_3. Subsequently, LDH are calcined at 773 K during 5 h to improve structural properties and texture, then a decarbonation and dehydration to obtain Mg–Fe–C with enhanced anionic exchange properties [25].

2.2.2. Preparation of organophilic LDH

Calcined LDH were added to a solution of surfactant, namely sodium dodecylsulfate (SDS, 0.1 M) with solid to solution ratio equal to 1 g/50 mL. The mixture constantly mixed and heated up to 338 K in an oil bath, while maintaining nitrogen reflux to minimize CO_3^{2-} amount in the solution

[26]. The resulting solid is washed five times with distilled water, then dried at 338 K and grinded to obtain Mg–Fe–SDS.

2.2.3. Preparation of humic acids

Commercially available humic acid (Acros) is used in the experiments. A solution with a concentration of 1 g/L is prepared by dissolving 1 g of humic acid in 62.5 mL of NaOH solution (2 N), followed by addition of distilled water to obtain 1l of solution. The latter is mixed during 24 h then filtered through a 45 μm filter and finally protected from light and kept at a temperature of 277 K [2,27].

2.3. Characterization

The samples isoelectric points are determined using the methodology described by Benhouria et al. [28]. In each Erlenmeyer flask, 50 mg of adsorbant are added to 50 mL of distilled water for a pH ranging between 2 and 12. The pH of each solution is adjusted by adding HCl or NaOH (0.01 M). The final pH is measured after 24 h of mixing. Morphological analysis using X-ray diffraction (XRD) is carried out using Bruker D8 diffractometer (40 kV, 30 mA), operating under copper monochromatic radiation ($K\alpha_{(\lambda Cu(K\alpha))}$ = 1.5406 Å). The domain of the 2θ angle observed ranges between 276 and 343 K. FTIR absorption spectra are recorded between 4,000 and 400 cm^{-1}, using a Fourier transform infrared spectrometer (FTIR) SHIMADZU FTIR 8400, with a resolution of 4 cm^{-1}. Texture measurement is performed using equipment of type accelerated surface area and porosimetry system (ASAP) 2010 (samples are degassed at 473 K and 0.1 Pa during 12 h before the adsorption analysis). Powder morphology was observed using Philips scanning electron microscopy (SEM) under 15 kV, which enables magnification of 30,000.

2.4. Effect of pH on adsorption

pH represents an important parameter for the adsorption process. It affects the charge of the adsorbent surface and the ionization of different functional groups as well as the adsorbate. The investigation of humic acid adsorption onto materials in seawater is carried out under pH values between 2 and 12. A mass of 10 mg of each material is added to 10 mL of solution with an initial concentration of 10 mg/L.

2.5. Adsorption kinetics of humic acid

The investigation of the kinetics of adsorption of a component onto an adsorbent enables to assess the influence of contact time on the adsorbed quantity [Eq. (1)]. The main objective of this research is to evaluate the time necessary to reach adsorption equilibrium for different concentrations. All results obtained are reported on a $Q_t = f(t)$ plot with:

$$Q_t = \frac{(C_0 - C_t)V}{m} \tag{1}$$

where C_0 is the initial concentration fo humic acid AH (mg/L), C_t is the residual concentration at time t (mg/L), V is the volume of the aqueous solution (L), and m the mass of clay (g).

2.6. Adsorption isotherm

Adsorption isotherms are drawn at room temperature using suspensions with 10 mg of adsorbent in 10 mL solutions with increasing humic acid concentration. The suspensions with pH = 5 are agitated during 6 h then centrifuged. The total equilibrium concentration of humic acid (C_e) is measured from the supernatant.

$$Q_e = \frac{(C_0 - C_e)V}{m} \tag{2}$$

where C_0 is the initial concentration of humic acid (mg/L), C_e is the residual equilibrium concentration (mg/L), V is the volume of the aqueous solution (L), and m is the mass of clay.

3. Results and discussions

3.1. Materials characterization

Results obtained from isoelectric points are reported on a ΔpH = $f(pH_i)$ plot (Fig. 1) where ΔpH = (pH_e – pH_i). The x-axis intercept of the curve indicates the value pH_{PZC}. The values of pH_{PZC} for Mg–Fe–SDS and Mg–Fe–C phases are 8.85 and 10.7, respectively [29].

Diffractograms of Mg–Fe–CO_3 sample, before calcination, after calcination, and after exchange by SDS are represented in Fig. 2. XRD results for Mg–F–CO_3 are typical of those of LDH structures encountered in the literature [30–32]. These symmetrical peaks at (003), (006), and (009), as well as asymmetrical at (015), (018), (110), and (113) indicate that our product is crystallized and similar to those reported in the literature [30]. Mg–Fe–C shows that calcination modifies the crystalline structure of LDHs by causing dehydration, dihydroxylation, and decarboxylation. Mixed oxides of MgO type are also formed at 2θ = 42°, 93° 62°, and 22°. These oxides, which are formed after calcination, are weakly crystallized and exhibit peak broadening on the XRD diagram in accordance with available literature [30–32]. After intercalation of SDS surfactant (Fig. 2), the crystalline structure reappears (memory effect) and shows characteristic peaks that correspond to initial LDH reflections. However, peak broadening points out, to some extent, a loss of crystallinity. The presence of SDS surfactant caused peak displacement towards small angles. The interreticular distances between (003) and (110) absorption bands allow the calculation of parameters a and c using $a = 2 \times d$ (110) and $c = 3 \times d$ (003). The interreticular distance of (003) band corresponds to the intersheet space while the absorption band (110) represents half the metal-metal distance in the sheet. The XRD parameters of the different samples are given in Table 1. All results are in accordance with reported values from the literature [30,31].

Mg–Fe–CO_3 diagram (Fig. 3) shows a wide band at ~3,440 cm^{-1}, which corresponds to a stretching vibration of lamellar hydroxide groups bonded to different metals [30,32]. A small vibration band observed at ~3,000 cm^{-1}corresponds to the stretching of water molecules [15,33]. A vibration band, observed at ~1,630 cm^{-1}, can be attributed to the deformation of interposed water molecules [30–32]. A vibration band around 1,353 cm^{-1}corresponds to asymmetric stretching of

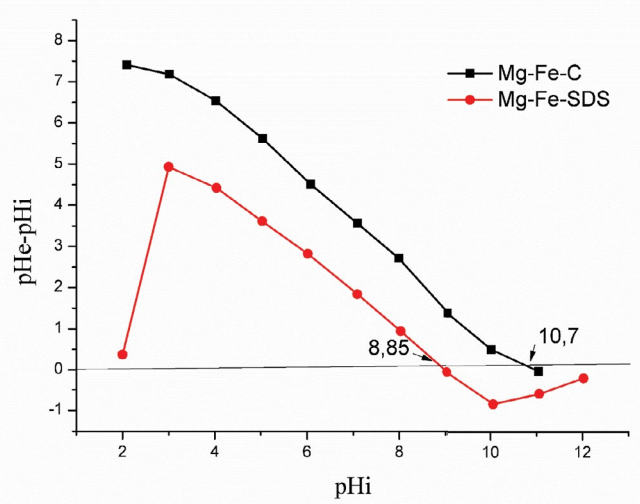

Fig. 1. Isoelectric points of the prepared materials.

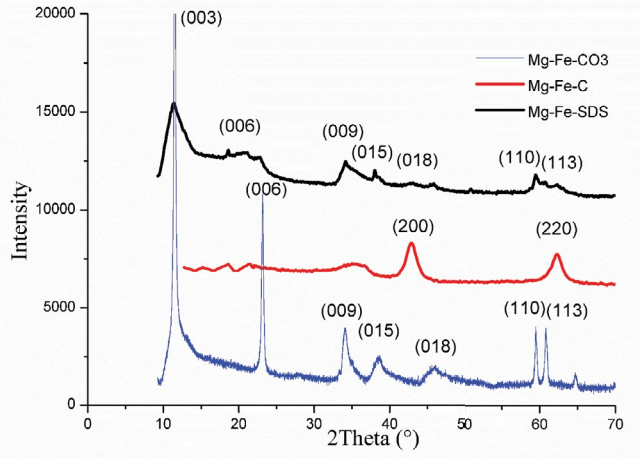

Fig. 2. XRD diagrams: Mg–Fe–CO_3, Mg–Fe–C, and Mg–Fe–SDS.

Table 1
Interlayer distance and lattice parameter for Mg–Fe–CO_3

	Mg–Fe–CO_3
d_{110}	1.55
A	3.1
d_{003}	7.6
d_{006}	13.85
d_{009}	2.63
C	22.83

interlamellar carbonates (CO_3^{-2}) [30,31]. Vibration bands in the range 800–500 $cm^{-1}$are attributed to valence vibrations of Mg–O, Fe–O [15,30,31,34]. IR spectra of calcined LDH at 773 K are represented in Fig. 3. Profiles analysis reveal a significant decrease in bands intensity at ~3,440 and ~1,630 cm^{-1}, which corresponds to a dihydroxylation and dehydration. Moreover, the disappearance of absorption peaks at ~3,000 and ~1,000 cm^{-1} can be attributed to surface decarboxylation.

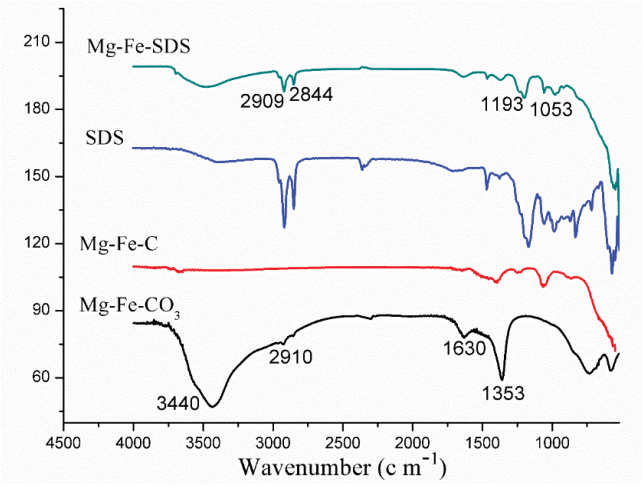

Fig. 3. IR spectra of anionic clays.

This phenomenon can lead to a decrease of the interlamellar distance. The presence of SDS ions in the interfoliar space is represented by the two peaks at ~2,909 and ~2,844 cm^{-1} for the Mg–Fe–SDS phase. These two peaks characterize both symmetric and asymmetric stretching of C–H bond that belongs to the linear chain of interposed SDS. The presence of sulfonate groups at ~1,053 cm^{-1} (ν (S=O) asymmetric) and~1,193 cm^{-1} (ν (S=O) symmetric) is also noticeable [35–37]. When anionic surfactants like dodecylsulfate are intercalated to LDH, the space between layers increases, and alteration of interlayer superficial properties from hydrophilic to hydrophobic occur. The hydrophobic nature and accessibility of the interlayer region of organocomposites make these materials promising candidates for adsorption of non-ionic organic pollutants. Anions (An^-) and interlayered water molecules can be exchanged for other anions, which makes LDH good anionic exchangers [35,38]. The adsorbent property of the LDH surface can be modified through the exchange of inorganic interlayered anions for organic anions such as anionic surfactants. We have used the anionic surfactant for the type of interaction that could exist between our materials and HA, interactions are of type electrostatic between the negatively charged sulfonate groups and the positive charges of HDL [35].

Nitrogen adsorption and desorption isotherms of calcined and non-calcined LDH at 77 K are represented in Fig. 4. The isotherms are of type IV following BDET (Brunauer, Deming, Emmet, and Teller) classification and the hysteresis loops are of type H_3. This adsorption isotherm is obtained with mesoporous adsorbents in which capillary condensation occurs [30]. It is observed from Table 2 that Brunauer–Emmett–Teller (BET) surfaces of calcined samples are greater than those of non-calcined samples, which is attributed to thermal treatment of the samples at 773 K. The elimination of water (dehydration) and carbon dioxide (decarbonation) during calcination can lead to channels and pores formation, which increases specific surface area of calcined samples in accordance with results from the literature [34,39]. The results obtained are in accordance.

SEM images show that non-calcined LDH are highly crystalline and reveal small porous particles in the shape

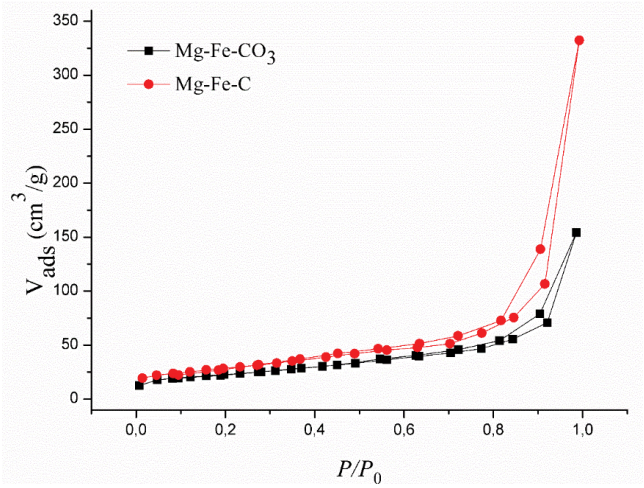

Fig. 4. Adsorption/desorption isotherms of anionic clays.

Table 2
BET parameters of prepared materials

Material	S_{BET} (m^2/g)	S_{ext} (m^2/g)	V_{pT} (cm^3/g)
Mg–Fe–CO_3	79	78.68	0.238
Mg–Fe–C	100.7	88.38	0.514

of platelets of average size. These particles are connected to each other in a textured arrangement [14]. Materials EDX elemental composition, illustrated by spectra of Fig. 5, shows the presence of different amounts of magnesium, iron, oxygen, and carbon. Regarding Mg–Fe–C, a decrease in oxygen and carbon is noticed which corresponds to surface dihydroxylation, dehydration, and decarboxylation, suggesting that calcination modifies LDH crystalline structure. These results confirm those obtained by XRD.

3.2. Effect of pH on adsorption

Carboxylic and phenolic groups confers to humic acid molecule a negative charge in aqueous solution. The adsorption of humic acid increases when pH is increased from 3 to 5 followed by a decrease for higher pH (Fig. 6). This is because the support attracts ions when pH values are lower than pHpzc [15], while for pH values higher than pHpzc, the support attracts cations. Therefore, when pH is high, there is repulsion with the anionic humic acid, which causes a decrease in adsorption further penalized by competition of humic acid ions with OH^- [2].

3.3. Effect of ionic force

The amount of humic acid adsorbed as a function of ions concentration in the solution (NaCl) is shown in Fig. 7. The investigation was carried out under the following operating conditions: C_0 = 10 mg/L, pH = 5, T = 298 K, V = 10 mL, m = 10 mg, $V_{agitation}$ = 200 tr/min. The adsorbed quantity for Mg–Fe–C decreases with the increase of the ionic force from 10^{-3} to 5.10^{-1} mol/L. This is attributed to two knowns causes [6,40], Firstly a competition between inorganic electrolyte (Cl^-) and humic acid adsorption on internal and external surfaces. Secondly, an increase in electrostatic attraction and ionic exchange between Cl^- ions, surface functions, and interlayer anions caused by an increase of the ionic force. NaCl has a weak effect during the adsorption of humic acid onto Mg–Fe–SDS for a humic acid concentration of 10 mg/L (Fig. 7). However, an increase of NaCl concentration causes a slight decrease in the percentage of elimination of humic acid. Nevertheless, an increase of the ionic force can cause a decrease in the molecular volume of humic acid due to the minimization of electrostatic repulsion between ionized oxygen groups [41,42]. Relatively small molecules are readily dispersed in the organic phase formed by long alkyl chains of dodecylsulfonate ions in the intermediate layer of organo-LDH [7].

3.4. Adsorption kinetics

Lagergren [43] proposed a first-order model that gives the evolution of adsorbed solute in time, viz:

$$Q_t = Q_e\left(1 - e^{-k_1 t}\right) \tag{3}$$

where k_1 represents the kinetic constant of the pseudo-first-order model (min^{-1}); Q_t is the instantaneous adsorption capacity (mg g^{-1}); Q_e is the equilibrium adsorption capacity (mg g^{-1}) and t is the time (min).

The pseudo-second-order equation was successfully used to describe adsorption kinetics of pollutants [44], viz:

$$Q_t = \frac{k_2\left(Q_e\right)^2 t}{1 + k_2 Q_e t} \tag{4}$$

where Q_t is the instantaneous adsorption capacity (mg g^{-1}); Q_e is the equilibrium adsorption capacity (mg g^{-1}); k_2 is the kinetic constant of pseudo-second-order model (g/mg min) and t is the time (min).

Intraparticle diffusion is generally expressed using Morris–Weber equation [45]:

$$Q_t = K_d t^{1/2} + C \tag{5}$$

With K_d the interparticle diffusion constant (mg/g $min^{0.5}$) or (mmol/g $min^{0.5}$); C is the y-axis intercept which represents the thickness of the boundary layer.

Comparison of the different models (Table 3) shows that the n-order ($n \in R^+$) $n \neq 1$ model gives the best fit of experimental data. Indeed, with a coefficient of determination r^2 = 0.99 and a negligible root mean square error, this model gives the best description of the adsorption process of humic acid on LDHs (Fig. 8). The model suggests an adsorption with charge interaction between adsorbent and adsorbate, a complex phenomenon that cannot be represented by a single parameter. Moreover, the calculated adsorbed amounts are in accordance with experimental values. Nevertheless, an order of 2 can be used as a first approximation during investigations of humic acid adsorption.

The model of intraparticle diffusion is used to further assess the adsorption mechanism of humic acid on

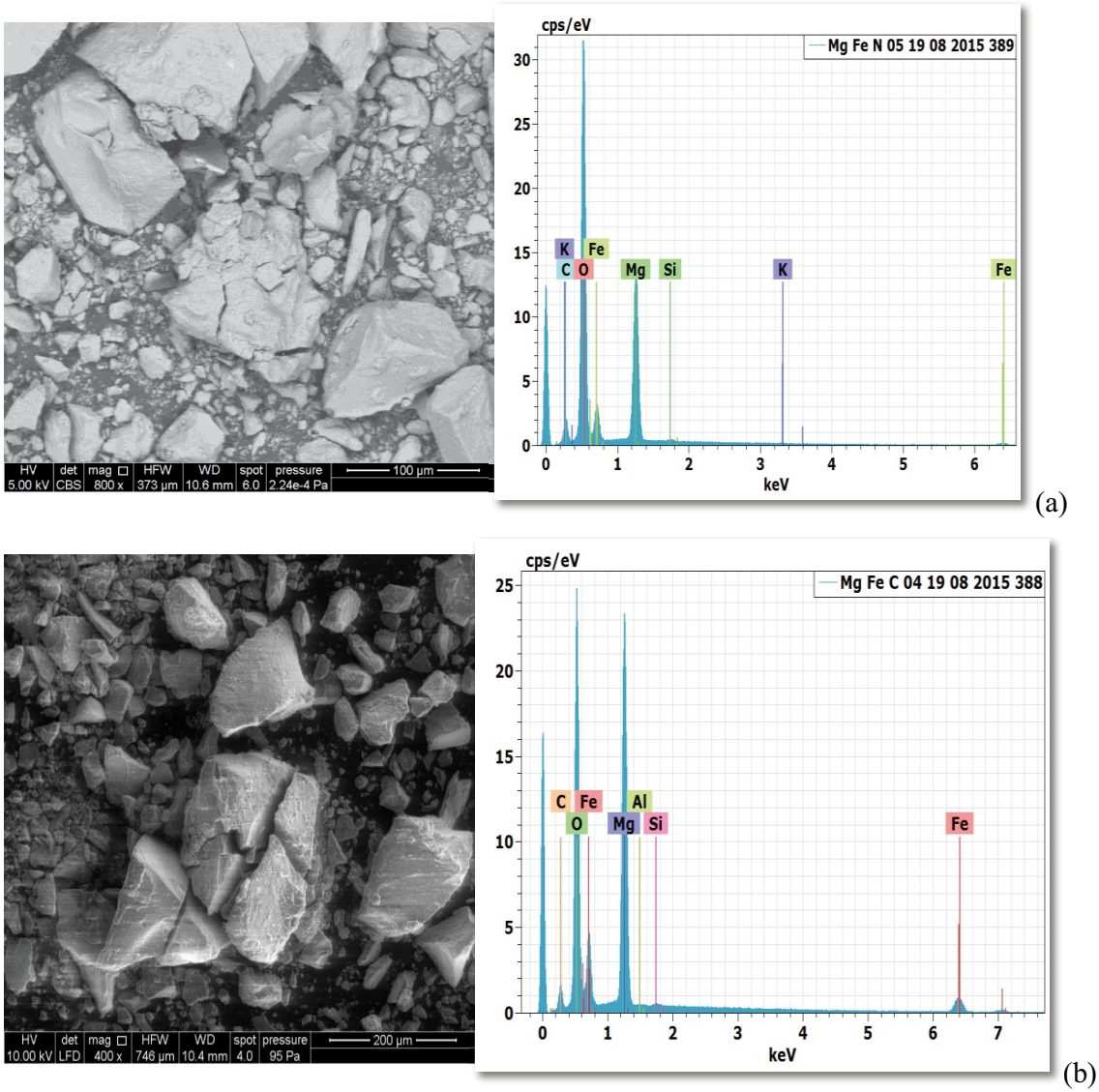

Fig. 5. SEM micrographs of prepared materials (a) Mg–Fe–CO_3 and (b) Mg–Fe–C.

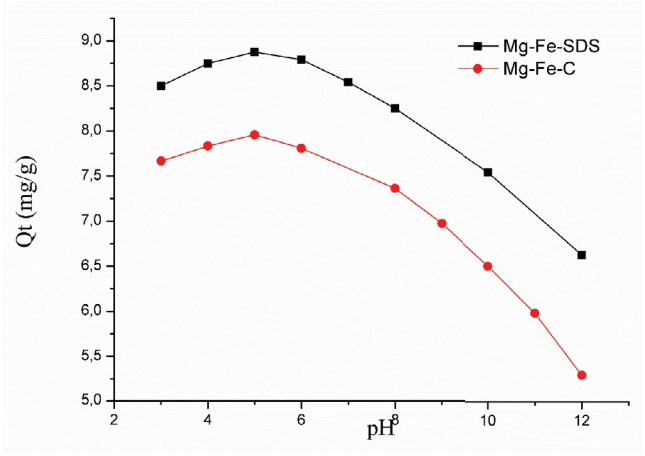

Fig. 6. Effect of pH on the adsorption of humic acid on prepared clays (C_0 = 10 mg/L, T = 298 K, and t = 5 h).

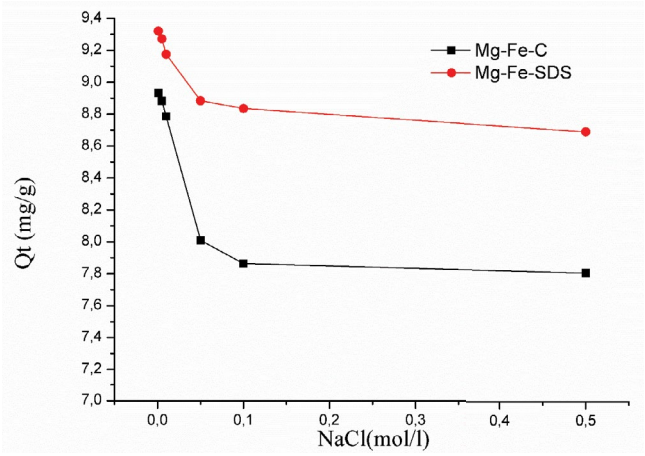

Fig. 7. Effect of ionic force on the adsorption of humic acid on LDHs in distilled water.

Table 3
Constants of adsorption kinetics models on different materials (C_0 = 10 mg/L, T = 298 K, pH = 5)

Models	Parameters	Mg–Fe–SDS			Mg–Fe–C			
		Initial concentrations (mg/L)						
		10	30	100	10	30	50	90
Pseudo-first-order model	Q_e(cal) (mg/g)	9	30	90	8	28	42	70
$q_t = q_e\left(1 - e^{-k_1 t}\right)$	RMSE	0.7268	1.6112	7.6039	0.3708	2.5974	2.5793	2.4560
	r^2	0.9354	0.9853	0.9332	0.9879	0.9435	0.9677	0.9896
	k_1 (min^{-1})	0.2100	0.1611	0.0763	0.0798	0.0899	0.1116	0.1349
Pseudo-second-order model	Q_e(cal) (mg/g)	8.66	29.85	88.78	7.88	27.63	41.72	69.62
	RMSE	0.3848	0.7559	3.6864	0.0811	1.4311	1.0807	0.9457
$Q_t = \frac{k_2\left(Q_e\right)^2 t}{1 + k_2 Q_e t}$	r^2	0.9771	0.9944	0.9765	0.9990	0.9768	0.9917	0.9976
	k_2 (g/mg/min)	0.0505	0.0143	0.0017	0.0173	0.0056	0.0073	0.0055
n-order model	Q_e(cal) (mg/g)	8.26	29.35	87.59	7.88	26.69	41.59	69.58
$Q_t = 1 - \left(1 + \left(n-1\right)k_n t\right)^{\frac{1}{1-n}}$	RMSE	0.1619	0.4090	3.2931	0.0809	0.8875	1.057	0.9420
	r^2	0.9936	0.9977	0.9804	0.9990	0.9885	0.9920	0.9977
	k_n	1.7028	1.7895	0.1992	0.1370	0.3451	0.3752	0.3601
	n	3.2940	2.9355	2.3430	1.9864	2.8749	2.1545	1.9428
Intraparticle diffusion	C	6.33	26.46	73.94	0.5	17.03	26.36	45.06
$Q_t = K_d t^{1/2} + C$	K	0.08	0.16	0.78	1.29	0.72	1.9	3.46
	r^2	0.834	0.879	0.841	0.901	0.965	0.900	0.991
Experimental value	Q_e(exp)	8.46	29.91	89.87	7.94	27.33	41.33	69.58

different materials. The amount adsorbed (Q_t) as a function of ($t^{0.5}$) for all samples exhibits three linear portions that do not cross the origin. This confirms that the intraparticle diffusion follows Morris–Weber model. However, intraparticular diffusion occurs simultaneously with other diffusion mechanisms. As can be seen in Fig. 9, the first sharper step was not observed and completed before 10 min, which may be considered as the external surface adsorption. The second linear portion corresponds the intra-particle diffusion and binding of molecules into the internal active sites of the LDH. Finally, the third linear portion indicated a saturation of the adsorption process [17,46].

The calculation of the parameters related to each model was carried out on MATLAB using genetic algorithms.

3.5. Adsorption isotherm

Langmuir isotherm has been used for the adsorption of a monolayer of solute onto a surface with finite number of identical sites. It assumes that adsorption energy is uniform over the entire surface [12,47]. It is generally expressed as:

$$Q_e = \frac{Q_m K_L C_e}{1 + K_L C_e} \tag{6}$$

with K_L the equilibrium constant, and Q_m the maximum adsorption capacity.

On the other hand, Freundlich model describes the adsorption equilibrium of solutes on heterogeneous surfaces. Therefore, this model assumes the presence of different types of adsorption sites and that solute adsorption can occur in a multilayer fashion. The model is generally described by the following equation [10,12]:

$$Q_e = K_F C_e^{1/n} \tag{7}$$

with Q_e is the adsorbed amount (mg/g), C_e is the equilibrium concentration (mg L^{-1}), K_F is the Freundlich coefficient, n is the solute affinity for the adsorbent.

Regarding Sips model, it extends Freundlich model to reach a limit for high concentrations [30]:

$$Q_e = \frac{Q_m K_s c_e^{\mathrm{ms}}}{1 + K_s c_e^{\mathrm{ms}}} \tag{8}$$

where K_s is Sips equilibrium constant (L/mmol). m_s is Sips model exponent.

By adjusting the experimental points on the different new models proposed with several parameters, and based on the values of the coefficient r^2 and RMSE, it appears that the values of the coefficient of correlations r^2 approaches unity and the RMSE tends toward zero, which clearly shows the precision of the models proposed compared to the Freundlich and Langmuir models. We also note that the adsorption process of HA on different materials is better presented by the proposed model (04) with four parameters (Table 4).

The adsorption of humic acids onto LDHs occurred by ion exchange with both the intercalated and surface anions of the LDH and ligand exchange reactions with surface groups. Lower molecular weight humic were preferentially adsorbed because these fractions can more easily enter the mesoporous LDHs and contain more carboxylic groups, which are known to be involved in ligand exchange reactions with, for example, surface groups. Intercalation of the entire HA molecules in-between the LDH sheets is

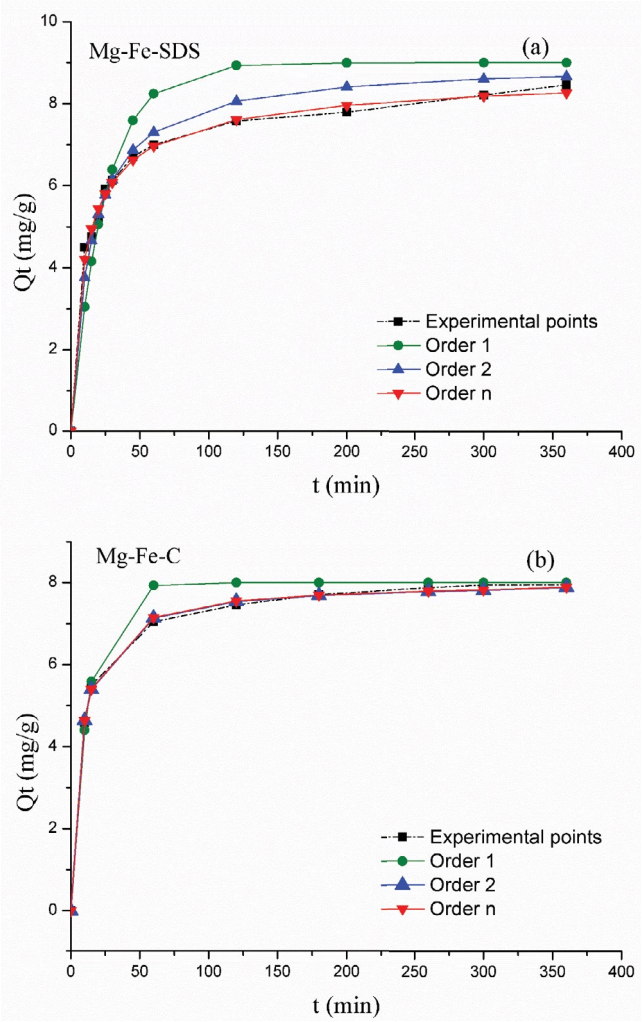

Fig. 8. Modeling of adsorption kinetics of humic acid on prepared clays (a) Mg–Fe–SDS and (b) Mg–Fe–C (C_0 = 10 mg/L).

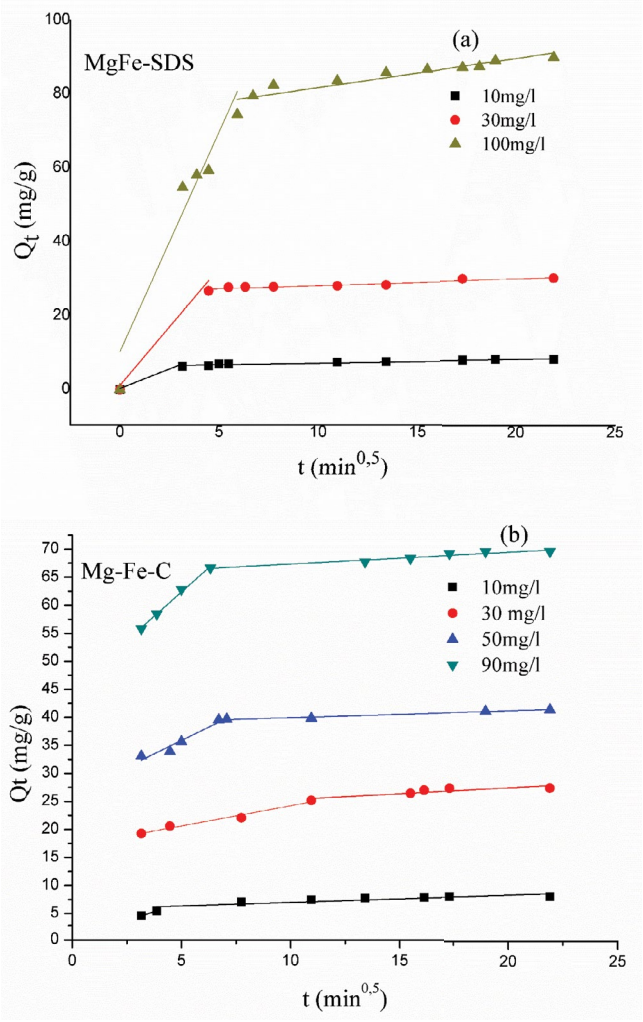

Fig. 9. Intraparticle diffusion model of Morris–Weber (a) Mg–Fe–SDS and (b) Mg–Fe–C.

unlikely to occur [48]. Curves of Fig. 10 shows the fitting of experimental data with these different models. The adsorption process of humic acid is well represented by the four parameters mode. Parameters calculation was performed on MATLAB using genetic algorithms.

3.6. Calculation of the effective diffusion coefficient and energy activation of adsorption for spherical adsorbent particles

In the absence of homogeneous chemical reaction, the unidimensional transient diffusion process of species (A) with a constant effective diffusion coefficient (D_A), in a homogeneous isotropic spherical adsorbent grain of radius (a), can be written as:

$$\frac{1}{a^2}\frac{\partial}{\partial a}\left(a^2 D_A \frac{\partial C_A}{\partial a}\right)-\frac{\partial C_A}{\partial t}=0 \tag{9}$$

Subject to the following boundary conditions:

$C_A(0,a) = C_0 = 0$, $C_A(t,a) = C_{AP} = C_{A0}$ and $C_A(t,0) = C_0 = 0$. With C_{AP} the concentration at the grain surface and C_{A0} the initial concentration of the solution.

The analytical solution of Eq. (9) subject to the above-mentioned boundary conditions is given by the method of separation of variables in the form of Fourier series, viz:

$$\frac{Q_{ad}^{e}(t)}{Q_{max}^{e}(t)}=1-\frac{6}{\pi^2}\sum_{n=1}^{\infty}\frac{1}{n^2}\exp\left(\frac{-n^2 D_A \pi^2}{a^2}t\right) \tag{10}$$

Where t represents the adsorption time and n is a positive integer.

Neglecting high order terms, Eq. (10) can be rewritten as:

$$\left(1-\frac{Q_{ad}^{e}(t)}{Q_{max}^{e}(t)}\right)=\frac{6}{\pi^2}\exp\left(\frac{-D_A \pi^2}{a^2}t\right) \tag{11}$$

Using logarithms on both sides of the Eq. (11):

$$\ln\left(1-\frac{Q_{ad}^{e}(t)}{Q_{max}^{e}(t)}\right)=\ln\left(\frac{6}{\pi^2}\right)-\left(\frac{D_A \pi^2}{a^2}\right)t \tag{12}$$

Table 4
Constants of adsorption isotherms of humic acid on different materials

Models	Parameters	Mg–Fe–SDS	Mg–Fe–C
Freundlich	RMSE	7.269	9.3987
$Q_e = K_F C_e^{1/n}$	r^2	0.9805	0.9409
	K_F	9.765	5.5297
	n	0.568	0.6552
	Q_m (rng/g)	153.9394	124.3548
Langmuir	RMSE	13.631	16.1161
$Q_e = \frac{Q_m K_L C_e}{1 + K_L C_e}$	r^2	0.9535	0.8844
	K_L	0.0402	0.0394
	Q_m (rng/g)	121.4834	90.23075
Sips	RMSE	6.9034	6.8806
$Q_e = \frac{Q_m K_s c_e^{ms}}{1 + K_s c_e^{ms}}$	r^2	0.9849	0.9712
	K_s	0.0036	0.0002
	n	1.6746	2.5072
	Q_m (rng/g)	134.0142	105.9268
Proposed model l	RMSE	4.4649	5.6142
$\frac{Q_e}{Q_m} = (1 - \exp(-aC_e^2))^{½}$	r^2	0.996	0.9835
	a	2.5629×10^{-04}	2.8598×10^{-04}
	Q_m (rng/g)	141.95	108.7987
Proposed model 2	RMSE	4.4377	4.9791
$\frac{Q_e}{Q_m} = b\ (1 - \exp(-aC_e^2))^{½}$	r^2	0.9956	0.984
	a	0.0003	2.356×10^{-4}
	b	0.9904	1.0685
	Q_m (mg/g)	140.74	115.0008
Proposed model 3	RMSE	2.9411	3.7993
$\frac{Q_e}{Q_m} = b\ (1 - \exp(-aC_e^n))^{½}$	r^2	0.997	0.9904
	a	0.0008	4.9814×10^{-5}
	b	1.041	1.0232
	n	1.6839	2.4518
	Q_m (*rng/g*)	143.82	112.3609
Proposed model 4	RMSE	2.684	3.212
$\frac{Q_e}{Q_m} = b\ (1 - \exp(-aC_e^n))^m$	r^2	0.9973	0.9927
	a	1.0033×10^{-05}	1.1699×10^{-07}
	b	1.0144	1.0021
	n	2.5967	3.8303
	m	0.281	0.2762
	Q_m (rng/g)	143	110.2307
Proposed model 5	RMSE	4.4303	4.7171
$\frac{Q_e}{Q_m} = 1 - \exp(-aC_e^n)$	r^2	0.9936	0.9856
	a	0.015	0.0026
	n	1.1207	1.6066
	Q_m (mg/g)	138.47	109.4338
Proposed model 6	RMSE	6.9034	6.8806
$\frac{Q_e}{Q_m} = (aC_e^n)/(1 + aC_e^n)$	r^2	0.9849	0.9712
	a	0.0036	0.0002
	n	1.6746	2.5071
	Q_m (mg/g)	145.41	105.9268
Experimental values	Q_m(exp)(mg/g)	142.33	109.32

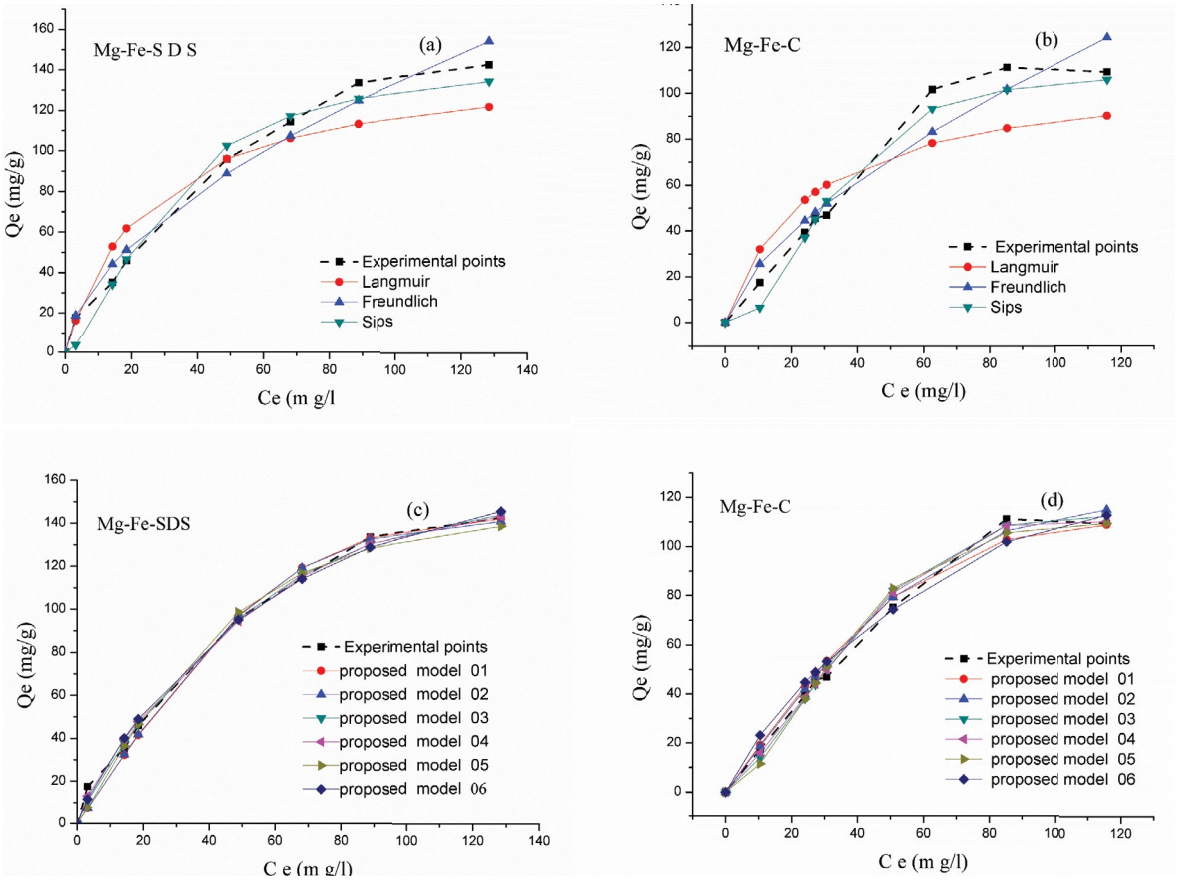

Fig. 10. Adsorption isotherms (a) Mg–Fe–SDS, (b) Mg–Fe–C, (c) Mg–Fe–SDS(proposed models), and (d) Mg–Fe–C (proposed models) (t = 5 h, T = 298 K, and C_0 = 10 mg/L).

Plotting $\left(1-\frac{Q_{ad}^{e}(t)}{Q_{max}^{e}(t)}\right)$ against (t), gives a straight line with a slope $\beta=\frac{D_A\pi^2}{a^2}$, which leads to a diffusion coefficient $D_A=\frac{\beta a^2}{\pi^2}$.

3.7. Calculation of the activation energy

It is assumed that the effective diffusion coefficient varies with temperature following an Arrhenius type equation, viz.

$$D_A=D_0\exp\left(-\frac{E_a}{R}\frac{1}{T}\right) \tag{13}$$

where D_0 is the Arrhenius pre-exponential factor, E_a is the activation energy of migration of adsorbate species (A). This energy characterizes the barrier to be overcome for species diffusion to occur at temperature (K).

Using logarithms on both sides of Eq. (13) leads to:

$$\ln\left(D_A\right)=\ln D_0-\left(\frac{E_a}{R}\frac{1}{T}\right) \tag{14}$$

The activation energy (E_a) is obtained from the slope of $\ln(D_A) = f(1/T)$ line. It is important to note that the weaker E_a the more efficient the adsorption.

The activation energy for each material can be calculated from values of the diffusion coefficient. This energy gives insight into whether the adsorption is chemical or physical. Results suggest that the adsorption process of humic acid is chemical for organophilic Mg–Fe and for Mg–Fe–C phase, with an activation energy of 28.26 kJ/mol and 32.73 kJ/mol, respectively. Similar results were reported by Santosa et al. [49] and Guo et al. [30]. Moreover, it is noticed that values of D_A lie within the range (10^{-13}–10^{-9}) m^2/s, and the higher the diffusion coefficient the more efficient the adsorption.

3.8. Effect of temperature on the adsorption process

The effect of temperature on the adsorption process was investigated by increasing temperature up to 313 K. As shown in Fig. 11, increasing the temperature causes an increase of the adsorbed amount of humic acid on both materials. Therefore, the adsorption process is endothermic, favored by relatively elevated temperatures [2].

3.9. Calculation of thermodynamic parameters

Values of Gibbs free energy ($\Delta G°$) of adsorption were calculated from enthalpy ($\Delta H°$) and entropy values,

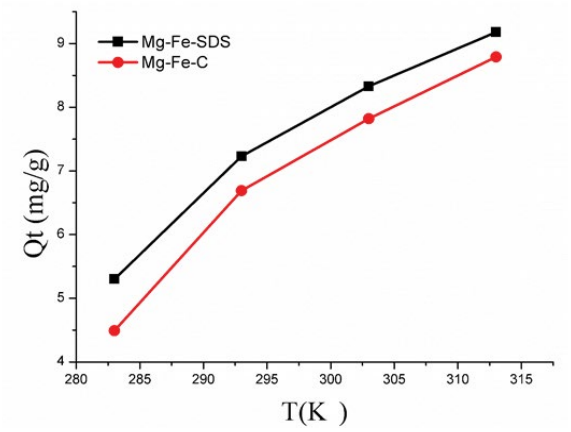

Fig. 11. Effect of temperature on the adsorption of humic acid on investigated clays.

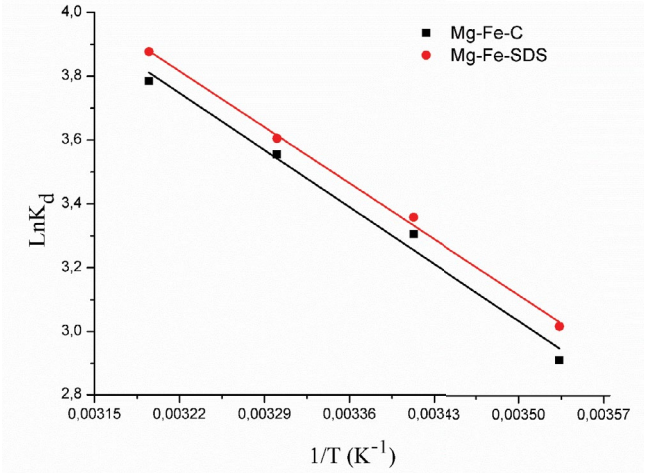

Fig. 12. Van't Hoff plot for different materials in seawater.

obtained from $\log(K_d \times 1{,}000) = f(1/T)$ plots of the following equations:

$$\Delta G^\circ = RT \ln K_d \tag{15}$$

$$\ln K_d = \frac{\Delta S^\circ}{T} - \frac{\Delta H^\circ}{RT} \tag{16}$$

$$\Delta G^\circ = \Delta H^\circ - T\Delta S^\circ \tag{17}$$

where K_d is the affinity of adsorption, and R the ideal gas constant.

Values of free energy ΔG°_{ads} reported in Table 5, suggest that the process is spontaneous while positive values of enthalpy ΔH° shows that the process is endothermic favored by increasing temperature (Fig. 12). Positive values of entropy ΔS°_{ads} show that LDH-adsorbate system is less ordered that the molecules of adsorbate in the liquid phase [2,31].

After absorption the spectrum of HA/Mg–Fe–SDS (Fig. 13) has peaks at 1,520.8 cm^{-1} [50], which are likely the stretching vibrations of –COO$^-$. The bands at 1,435.5 and 1,150.0 cm^{-1} correspond to –COO– vibrations and C–O stretching vibrations, respectively [51]. The peaks at 790.3 cm^{-1} represent the aromatic C–H stretching vibrations [21,49]. In addition, the bands at 672.5, 610.0, and 558.8 cm^{-1}, which are located in the region of 450–750 cm^{-1}, all represented Al–O and Mg–O vibrations [22]. The vibration bands at 419.8 cm^{-1} appeared for the HA/Mg–Fe–SDS, corresponding to the aromatic C–H vibration, which may be derived from humic acid at 452.6 cm^{-1} [22]. These results indicated that the absorption of humic acid on the surface and layer of Mg–Fe–SDS had occurred, and the interactions such as van der Waals forces, hydrogen bonding, and electrostatic attraction had existed between the Mg–Fe–SDS layers and humic acid molecules.

The morphological features of the Mg–Fe–SDS after sorption of humic acid are shown in Fig. 14. After the sorption of HA, the material aggregated; the layer thickness increased obviously, and the material formed a shale-like layered structure. It also can be seen from Fig. 14 that there are some plate-like areas left on the surface, which are similar to the raw Mg–Fe–SDS. This may because the sorption was unsaturated, leaving some areas unoccupied by HA [7]. According to the literature, the different types of interactions between surfactants and surface of LDHs are the first type (type I) are electrostatic forces between the positive charges of LDH and the negative charges of sulfonate groups of the surfactant. The second type is the interactions of the bond hydrogen between the sulfonate

Table 5
Thermodynamic parameters ΔH°, ΔS°, and ΔG° related to the adsorption of Mg–Fe–SDS and Mg–Fe–C

Samples	Temperature (K)	ΔG° (kJ/mol)	ΔH° (kJ/mol)	ΔS° (kJ/mol k)
Mg–Fe–SDS	283	–16.42	47.98	22.75
	293	–18.69		
	303	–20.97		
	313	–23.24		
Mg–Fe–C	283	–16.02	48.83	22.91
	293	–18.31		
	303	–20.6		
	313	–22.95		

Table 6
Comparison of monolayer adsorption of HA onto various adsorbents

Adsorbents	q_{max} (mg/g)	References
Mg/Fe layered double hydroxide	76.70	[6]
Palygorskite	17	[53]
Acid-activated Greek bentonite	12.062	[41]
Polyaniline/attapulgite composite	61.35	[54]
Crosslinked chitosan-epichlorohydrin beads	44.84	[55]
Chitosan treated granular activated carbon	71.4	[56]
Hexadecyltrimethyl ammonium bromide (HTAB)-modified zeolite synthesized from coal fly ash	126.6	[57]
Mg/Al layered double hydroxide	69	[49]
HDL–DSO	594.3	[7]
Mg–Fe–SDS	142.33	This study
Mg–Fe–C	109.32	This study

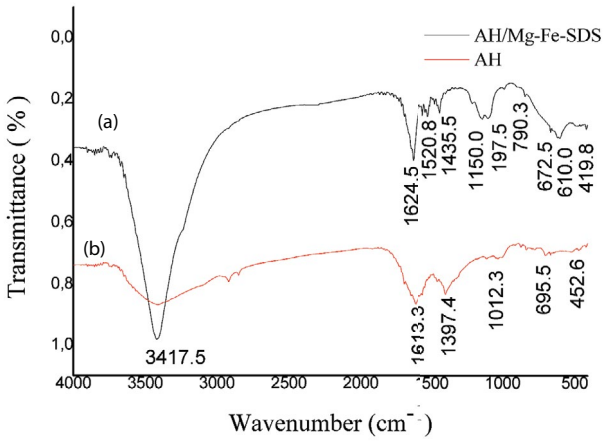

Fig. 13. FTIR spectra after adsorption of HA/Mg–Fe–SDS (a) and humic acid (b).

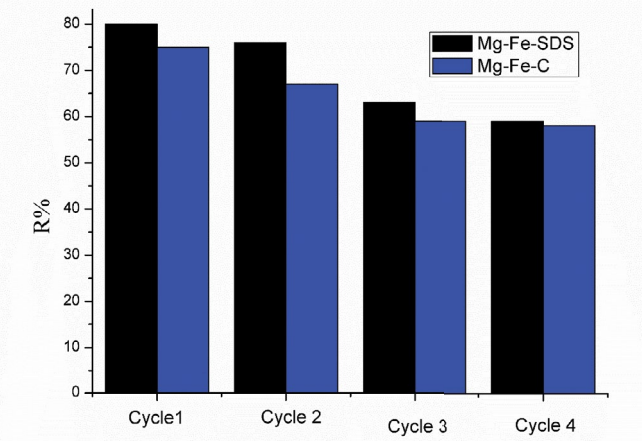

Fig. 15. Histogram of materials regeneration in seawater (C_0 = 10 mg/L and T = 298 K).

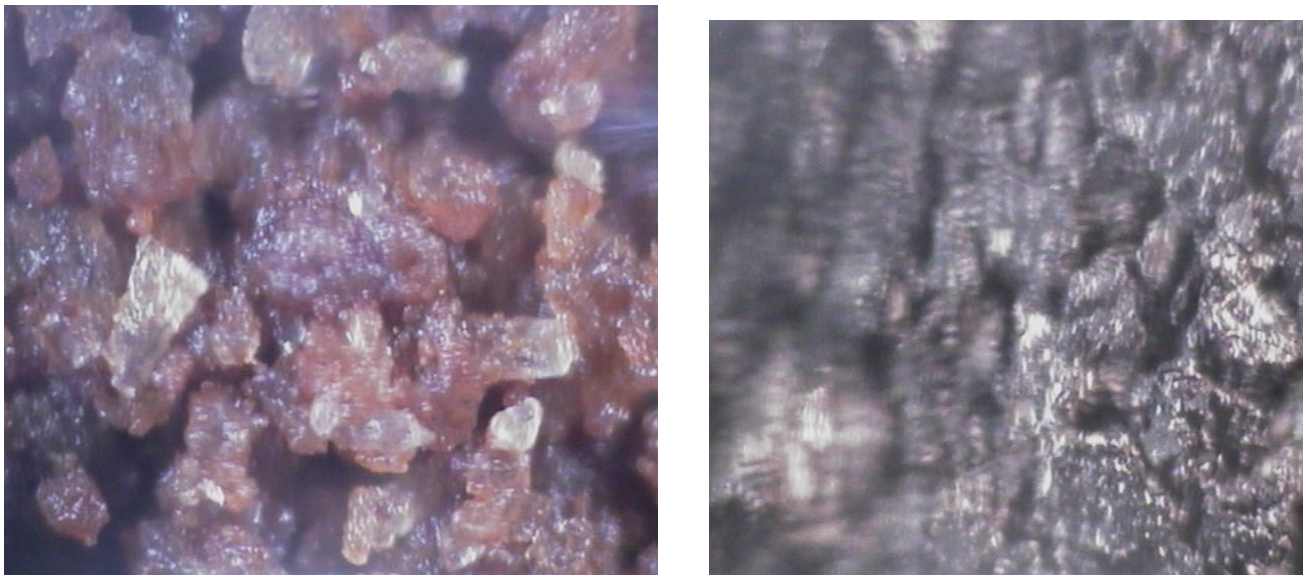

Fig. 14. Scanning electron micrographs of (a) Mg–Fe–SDS after sorption of HA and (b) humic acid.

groups and the hydroxyl groups of LDH (type II) which is combined with hydrophobic interactions between the CH_2 groups of the surfactant (type III) [52].

3.10. Regeneration

Regeneration of the adsorbent is an important economical factor in treatment processes. Focus is generally set on the regeneration mechanism and recycling of adsorbents charged with pollutants. Small quantities of humic acid adsorbed on calcined LDH and organophilic LDH at high pH imply that the adsorbent charged with humic acid can be desorbed in alkaline medium. A regeneration analysis was carried out after adsorption using NaOH 0.1 M [3] and the materials obtained were reused for adsorption. The throughput of the elimination process was determined after several experiments. After each cycle, the adsorbed quantity is calculated using Eq. (1) with C_0 = 10 mg/L. The results of regeneration are reported in the histogram of Fig. 15. It is noted that after the first cycle, the adsorption capacity of humic acid decreases from 80% to 76% compared to the original Mg–Fe–SDS and from 75% to 67% compared to original Mg–Fe–C. Therefore, the decrease in adsorption capacity is low, which gives the materials an excellent regeneration property.

4. Conclusion

Materials characterization confirmed successful synthesis of LDHs. Results of infrared spectra showed LDH characteristic bands with carbonate anions interposed in the interlamellar spacing. Thermal treatment confers to the material a relatively high specific surface. SEM and XRD characterization results show that LDH are crystalline. This crystalline structure reappears (memory effect) after interposing SDS surfactant in LDHs with characteristic peaks that correspond to initial LDH reflections with a slight modification of crystallinity.

Results show that pseudo-first-order kinetic model is valid at early stages of the adsorption process, while the pseudo-second-order model gives better results. However, the best fit of the experimental results was obtained using the *n*-order model ($n \in R^+$) $n \neq 1$ with a determination coefficient close to one. Models of adsorption isotherms that were proposed, particularly 4 parameters model, give better results than classical Freundlich, Langmuir, and Sips models. Calculated effective diffusion coefficient and activation energies are in accordance with values reported in the literature. A thermodynamics analysis enabled the calculation of enthalpy, entropy, and free energy of adsorption and showed that the adsorption process is chemical, spontaneous, and endothermic (Table 6). Finally, the prepared materials were regenerated and reused successfully in several successive adsorption cycles.

References

[1] R.S. Gabor, K. Eilers, D.M. McKnight, N. Fierer, S.P. Anderson, From the litter layer to the saprolite: chemical changes in water-soluble soil organic matter and their correlation to microbial community composition, Soil Biol. Biochem., 68 (2014) 166–176.
[2] H.D. Bouras, O. Benturki, N. Bouras, M. Attou, A. Donnot, A. Merlin, F. Addoun, M.D. Holtz, The use of an agricultural waste material from *Ziziphus jujuba* as a novel adsorbent for humic acid removal from aqueous solutions, J. Mol. Liq., 211 (2015) 1039–1046.
[3] T.S. Anirudhan, M. Ramachandran, Surfactant-modified bentonite as adsorbent for the removal of humic acid from wastewaters, Appl. Clay Sci., 35 (2007) 276–281.
[4] J. Wang, Y. Zhou, A. Li, L. Xu, Adsorption of humic acid by bi-functional resin JN-10 and the effect of alkali-earth metal ions on the adsorption, J. Hazard. Mater., 176 (2010) 1018–1026.
[5] Y. Zhang, X. Zhang, Y. Song, J. Wang, Enhanced performance of calcium-enriched coal ash for the removal of humic acids from aqueous solution, Fuel, 141 (2015) 93–98.
[6] M.S. Gasser, H.T. Mohsen, H.F. Aly, Humic acid adsorption onto Mg/Fe layered double hydroxide, Colloids Surf., A, 331 (2008) 195–201.
[7] G. Zhang, T. Wu, Y. Li, X. Huang, Y. Wang, G. Wang, Sorption of humic acid to organo layered double hydroxides in aqueous solution, Chem. Eng. J., 191 (2012) 306–313.
[8] J. Liu, J. Cao, H. Chen, D. Zhou, Adsorptive removal of humic acid from aqueous solution by micro and mesoporous covalent triazine based framework, Colloids Surf., A, 481 (2015) 276–282.
[9] S. Kumpulainen, F. von der Kammer, T. Hofmann, Humic acid adsorption and surface charge effects on schwertmannite and goethite in acid sulphate waters, Water Res., 42 (2008) 2051–2060.
[10] S. Bousba, N. Bougdah, N. Messikh, P. Magri, Adsorption removal of humic Acid from water using a modified Algerian bentonite, Phys. Chem. Res., 6 (2018) 613–625.
[11] J. Lin, Y. Zhan, Adsorption of humic acid from aqueous solution onto unmodified and surfactant-modified chitosan/zeolite composites, Chem. Eng. J., 200–202 (2012) 202–213.
[12] F. Gomri, M. Boutahala, H. Zaghouane-Boudiaf, S.A. Korili, A. Gil, Removal of acid blue 80 from aqueous solutions by adsorption on chemical modified bentonites, Desal. Water Treat., 57 (2016) 26240–26249.
[13] K. Morimoto, Determination and reduction of Fe(III) incorporated into Mg–Fe layered double hydroxide structures, Appl. Clay Sci., 121–122 (2016) 71–76.
[14] Q. Xu, Y. Wei, Y. Liu, X. Ji, L. Yang, M. Gu, Preparation of Mg/Fe spinel ferrite nanoparticles from Mg/Fe-LDH microcrystallites under mild conditions, Solid State Sci., 11 (2009) 472–478.
[15] I.M. Ahmed, M.S. Gasser, Adsorption study of anionic reactive dye from aqueous solution to Mg–Fe–CO_3layered double hydroxide (LDH), Appl. Surf. Sci., 259 (2012) 650–656.
[16] F.L. Theiss, G.A. Ayoko, R.L. Frost, Synthesis of layered double hydroxides containing Mg^{2+}, Zn^{2+}, Ca^{2+} and Al^{3+} layer cations by co-precipitation methods – a review, Appl. Surf. Sci., 383 (2016) 200–213.
[17] C. Tiar, M. Boutahala, A. Benhouria, H. Zaghouane-Boudiaf, Synthesis and physicochemical characterization of ZnMgNiAl–CO_3-layered double hydroxide and evaluation of its sodium dodecylbenzenesulfonate removal efficiency, Desal. Water Treat., 57 (2016) 13132–13143.
[18] M. Cruz-Guzman, R. Celis, M.C. Hermosin, J. Cornejo, Adsorption of the herbicide sinezine by montmorillonite modified with neutral organic cations, Environ. Sci. Technol., 38 (2004) 180–186.
[19] S. Li, Y. Yang, S. Huang, Z. He, C. Li, D. Li, B. Ke, C. Lai, Q. Peng, Adsorption of humic acid from aqueous solution by magnetic Zn/Al calcined layered double hydroxides, Appl. Clay Sci.,180 (2020) 105414.
[20] F. Zermane, B. Cheknane, J.P. Basly, O. Bouras, M. Baudu, Influence of humic acids on the adsorption of Basic Yellow 28 dye onto an iron organo–inorgano pillared clay and two hydrous ferric oxide, J. Colloid Interface Sci., 395 (2013) 212–216.
[21] Y. Xiang, F. Kang, Y. Xiang, Y. Jiao, Effects of humic acid-modified magnetic Fe_3O_4/MgAl-layered double hydroxide on the plant growth, soil enzyme activity, and metal availability, Ecotoxicol. Environ. Saf.,182 (2019) 109424.
[22] M. Shi, Z. Zhao, Y. Song, M. Xu, J. Li, L. Yao, A novel heat-treated humic acid/ MgAl-layered double hydroxide composite for efficient removal of cadmium: fabrication, performance and mechanisms, Appl. Clay Sci., 187 (2020) 105482.

[23] R. Lafi, K. Charradi, M.A. Djebbi, A.B. Haj Amara, A. Hafiane, Adsorption study of Congo red dye from aqueous solution to Mg–Al–layered double hydroxide, Adv. Powder Technol., 27 (2016) 232–237.
[24] R. Chitrakar, S. Tezuka, A. Sonoda, K. Sakane, K. Ooi, T. Hirotsu, Adsorption of phosphate from seawater on calcined MgMn-layered double hydroxides, J. Colloid Interface Sci., 290 (2005) 45–51.
[25] W.T. Reichle, Synthesis of anionic clay minerals (mixed metal hydroxides hydrotalcite), Solid State Ionics, 22 (1986) 135–141.
[26] Y. You, H. Zhao, G.F. Vance, Surfactant-enhanced adsorption of organic compounds by layered double hydroxides, Colloids Surf., A, 205 (2002) 161–172.
[27] F. Zermane, M.W. Naceur, B. Cheknane, N. Ait Messaoudene, Adsorption of humic acids by a modified Algerian montmorillonite in synthesized seawater, Desalination, 179 (2005) 375–380.
[28] A. Benhouria, M.A. Islama, H. Zaghouane-Boudiaf, M. Boutahala, B.H. Hameed, Calcium alginate–bentonite–activated carbon composite beads as highly effective adsorbent for methylene blue, Chem. Eng. J., 270 (2015) 621–630.
[29] A. Halajnia, S. Oustan, N. Najafi, A.R. Khataee, A. Lakzian, The adsorption characteristics of nitrate on Mg–Fe and Mg–Al layered double hydroxides in a simulated soil solution, Appl. Clay Sci., 70 (2012) 28–36.
[30] Y. Guo, Z. Zhu, Y. Qiu, J. Zhao, Enhanced adsorption of acid brown 14 dye on calcined Mg/Fe layered double hydroxide with memory effect, Chem. Eng. J., 219 (2013) 69–77.
[31] N. Benselka-Hadj Abdelkader, A. Bentouami, Z. Derrich, N. Bettahar, L.C. de Ménorva, Synthesis and characterization of Mg–Fe layer double hydroxides and its application on adsorption of Orange G from aqueous solution, Chem. Eng. J., 169 (2011) 231–238.
[32] H. Murase, H. Yasuda, A. Nakahira, Effect of high magnetic field on ferrite materials obtained by calcination of layered double hydroxide, Mater. Trans., 48 (2007) 2877–2882.
[33] M.J. Reis, F. Silverio, J. Tronto, J.B. Valim, Effects of pH, temperature, and ionic strength on adsorption of sodium dodecylbenzenesulfonate into Mg–Al–CO_3 layered double hydroxides, J. Phys. Chem. Solids, 65 (2004) 487–492.
[34] F.P. Jiao, L. Shuai, J.G. Yu, X.Y Jiang, X.Q. Chen, S.L. Du, Adsorption of glutamic acid from aqueous solution with calcined layered double Mg–Fe–CO_3 hydroxide, Trans. Nonferrous Met. Soc. China, 24 (2014) 3971–3978.
[35] L.D.L. Miranda, C.R. Bellato, M.P.F. Fontes, M.F. de Almeida, J.L. Milagres, L.A. Minim, Preparation and evaluation of hydrotalcite-iron oxide magnetic organo composite intercalated with surfactants for cationic methylene blue dye removal, Chem. Eng. J, 254 (2014) 88–97.
[36] X. Ruan, S. Huang, H. Chen, G. Qian, Sorption of aqueous organic contaminant sonto dodecyl sulfate intercalated magnesium iron layered double hydroxide, Appl. Clay Sci., 72 (2013) 96–103.
[37] P. Zhang, T. Wang, G. Qian, D. Wu, R.L. Frost, Effective intercalation of sodium dodecylsulfate (SDS) into hydrocalumite: mechanism discussion via near-infrared and mid-infrared investigations, Spectrochim. Acta, Part A, 149 (2015) 166–172.
[38] F. Bruna, R. Celis, M. Real, J. Cornejo, Organo/LDH nanocomposite as an adsorbent of polycyclic aromatic hydrocarbons in water and soil–water systems, J. Hazard. Mater., 225–226 (2012) 74–80.
[39] B. Hudcová, M. Vítková, P. Ouředníček, M. Komárek, Stability and stabilizing efficiency of Mg–Fe layered double hydroxides and mixed oxides in aqueous solutions and soils with elevated As(V), Pb(II) and Zn(II) contents, Sci. Total Environ., 648 (2019) 1511–1519.
[40] S. Miyata, Anion-exchange properties of hydrotalcite-like compounds, Clays Clay Miner., 31 (1983) 305–311.
[41] D. Doulia, C. Leodopoulos, K. Gimouhopoulos, F. Rigas, Adsorption of humic acid on acid-activated Greek bentonite, J. Colloid Interface Sci., 340 (2009) 131–141.
[42] X. Peng, Z. Luan, H. Zhang, Montmorillonite–Cu(II)/Fe(III) oxides magnetic materialas adsorbent for removal of humic acid and its thermal regeneration, Chemosphere, 63 (2006) 300–306.
[43] S.Y. Lagergren, On the theory of so-called adsorption of solutes, K. Sven. Vetenskapsakad. Handl., 24 (1898) 1–39.
[44] Y.S. Ho, G. McKay, Pseudo-second-order model for sorption processes, Process Biochem., 34 (1999) 451–465.
[45] W.J. Weber, J.C. Morris, Kinetics of adsorption on carbon from solution, J. Sanitary Eng. Div., 89 (1963) 31–60.
[46] B.H. Hameed, I.A.W. Tan, A.L. Ahmad, Adsorption isotherm, kinetic modeling and mechanism of 2,4,6-trichlorophenol on coconut husk-based activated carbon, Chem. Eng. J., 144 (2008) 235–244.
[47] A.W.M. Ip, J.P. Barford, G. McKay, Reactive black dye adsorption/desorption onto different adsorbents: effect of salt, surface chemistry, pore size and surface area, J. Colloid Interface Sci., 337 (2009) 32–38.
[48] S. Vreysen, A. Maes, Adsorption mechanism of humic and fulvic acid onto Mg/Al layered double hydroxides, Appl. Clay Sci., 38 (2008) 237–249.
[49] S.J. Santosa, E.S. Kunarti, Karmanto, Synthesis and utilization of Mg/Al hydrotalcite for removing dissolved humic acid, Appl. Surf. Sci., 254 (2008) 7612–7617.
[50] J. Sun, Y. Chen, H. Yu, L. Yan, B. Du, Z. Pei, Removal of Cu^{2+}, Cd^{2+} and Pb^{2+} from aqueous solutions by magnetic alginate microsphere based on Fe_3O_4/MgAl-layered double hydroxide, J. Colloid Interface Sci., 532 (2018) 474–484.
[51] Z. Wang, X. Zhang, H. Zhang, G. Zhu, Y. Gao, Q. Cheng, X. Cheng, Synthesis of magnetic nickel ferrite/carbon sphere composite for levofloxacin elimination by activation of persulfate, Sep. Purif. Technol., 215 (2019) 528–539.
[52] D. Li, X. Xu, J. Xu, W. Hou, Poly(ethylene glycol) haired layered double hydroxides as biocompatible nanovehicles: morphology and dispersity study, Colloid Surf., A, 384 (2011) 585–591.
[53] M.S. Wang, L.B. Liao, X.L. Zhang, Z.H. Li, Adsorption of low concentration humic acid from water by palygorskite, Appl. Clay Sci., 67–68 (2012) 164–168.
[54] J.H. Wang, X.J. Han, H.R. Ma, Y.F. Ji, L.J. Bi, Adsorptive removal of humic acid from aqueous solution on polyaniline/attapulgite composite, Chem. Eng. J., 173 (2011) 171–177.
[55] W.S. Wan Ngah, M.A.K.M. Hanafiah, S.S. Yong, Adsorption of humic acid from aqueous solutions on crosslinked chitosan-epichlorohydrin beads: kinetics and isotherm studies, Colloid Surf., B, 65 (2008) 18–24.
[56] S. Maghsoodloo, B. Noroozi, A.K. Haghi, G.A. Sorial, Consequence of chitosan treating on the adsorption of humic acid by granular activated carbon, J. Hazard. Mater.,191 (2011) 380–387.
[57] C.J. Li, Y. Dong, D.Y. Wu, L.C. Peng, H.N. Kong, Surfactant modified zeolite as adsorbent for removal of humic acid from water, Appl. Clay Sci., 52 (2011) 353–357.